Combustion and Flame 215 (2020) 333–341

Contents lists available at ScienceDirect

Combustion and Flame

journal homepage: www.elsevier.com/locate/combustflame

Learning-based prediction of wildfire spread with real-time rate of spread measurement

Chunjie Zhai[a,b,*], Siyu Zhang[c,**], Zhaolou Cao[d], Xinmeng Wang[a]

[a] Department of Information Technology, Nanjing Forest Police College, Nanjing 210023, China
[b] College of Safety Science and Engineering, Nanjing Tech University, Nanjing 210009, China
[c] Department of Forest Fire Protection, Nanjing Forest Police College, Nanjing 210046, China
[d] School of Physics and Optoelectronic Engineering, Nanjing University of Information Science and Technology, Nanjing 210044, China

ARTICLE INFO

Article history:
Received 8 June 2019
Revised 14 October 2019
Accepted 6 February 2020
Available online 28 February 2020

Keywords:
Wildfire spread
Real-time RoS measurement
Level-set method
Machine learning

ABSTRACT

A learning-based wildfire spread model was developed in this study to predict short-term wildfire spread. Real-time rate of spread (RoS) measurement was first conducted by calculating normal movements of fire fronts. Subsequently, machine learning was employed to correlate the local RoS and environmental parameters and predict the RoS in the unburnt area. After that, a narrow-band level-set method was utilized to simulate the evolution of fire front. RoS measurement, machine learning, and level-set method were individually verified with numerically generated fire fronts, and applied in a real scale shrubland fire scenario. Results show that the proposed learning-based method is capable of predicting short-term fire spread without employing an empirical RoS model, which is beneficial for modeling spreading of a real wildfire.

1. Introduction

Wildfire usually occurs in countryside or rural area unexpectedly and accidently. As it leads to great human casualties, environmental and economic losses every year all over the world, its characteristics and prevention attracts much attention in fire safety community for decades [1–6]. Accurate prediction of wildfire spread would be helpful in developing suitable fire control plans to reduce the risk. However, prediction based on empirical knowledge still plays an important role in fire prevention nowadays, especially in developing countries. An accurate and computationally practical numerical wildfire spread model that provides useful information in a timely manner is a crucial part for wildfire prediction, which has been a goal of the fire research community for a long time. Two types of numerical wildfire spread models are generally used in the literature. The first one is based on physical modeling accounting for various physical and chemical phenomena, like computational-fluid-dynamics (CFD) models [7–9]. Although the models work well for laboratory experiments and controlled field-scale experiments, further improvements are still required to simulate a real wildfire due to complicated environments and high computational costs. The other one relies on empirical models of rate of spread (RoS) that correlate RoS, slope, wind, and vegetation properties [10–17], which has been employed in the well-known wildfire simulation tool FARSITE [10]. The empirical model simplifies the overall combustion processes but employs a RoS expression based on empiric knowledge for given environments. It has been widely used in real-time wildfire spread prediction since it is computationally efficient. As no empirical RoS model can perfectly predict a real wildfire spread, the model results only agree with experimental observation in a localized region within a period. Detailed discussion about uncertainties associated with model predictions of RoS for surface and crown fire was given in Cruz et al. [16], showing that only 3% of the predictions (i.e., 35 out of 1278) were considered to be exact predictions. Therefore, an empirical RoS model with improved accuracy is necessary for modeling wildfire spreading.

Data-driven simulation is a well-established approach in various applications [18–20], showing its ability to reduce simulation uncertainty. Facilitated by the development of unmanned aerial vehicle, imaging of real-time fire scenes with large field-of-view and high spatial resolution is now available in most cases [21–23]. Although there is still a lot of work to do for more accurate location of fire fronts from infrared remote sensing im-

* Corresponding author at: Department of Information Technology, Nanjing Forest Police College, Nanjing 210023, China.
** Corresponding author.
E-mail addresses: zhaichunjie1988@163.com (C. Zhai), siyu85878817@163.com (S. Zhang).

https://doi.org/10.1016/j.combustflame.2020.02.007
0010-2180/

agery, several works have already been conducted to update RoS model parameters with extracted fire fronts for the prospects in data-driven wildfire spread modeling. Mandel et al. [24,25] first employed this data-driven method in predicting of flame temperature and location with Kalman filter and atmosphere-coupled wildfire spread model. Rochoux et al. [26–28] extended their work by exploring a data-driven fire spread model that adjusts model parameter based on fire front measurements. The model was validated in controlled small-scale and field-scale experiments. As the model can work in a parallel running strategy, it shows high computational efficiency. Genetic algorithms were adopted by Denham et al. [29] and Lautenberger [30] for global optimization of model parameter, demonstrating its capability of calibrating model parameters. Lagrangian framework tracking front markers individually was used by Rios et al. [31,32] as an alternate approach of level set method in above works to reduce the grid dependency, which was validated by short-term fire front spread prediction of controlled shrubland fire. In these works, the deviation between predicted and observed of fire front was minimized by optimizing the parameters of an explicit empirical RoS model. However, it is usually difficult to determine which RoS model should be employed in a real wildfire. Consequently, an approach avoiding the use of empirical RoS model is desirable, which is the motivation of this work. In recent years, machine learning has attracted much attention for its ability to learn nonlinear relationship among various parameters. It inspires us to apply machine learning in RoS modeling to solve the aforementioned issue. As predicting fire fronts from raw observed fire fronts requires a large-scale neural network, we firstly calculate the RoS from observed fire fronts and then utilize machine learning to obtain the dependence of RoS on related parameters based on reliable RoS measurements, which could greatly reduce the complexity of neural network.

In this work, a data-driven wildfire spread model is systematically studied based on machine learning with assumption of available fire front positions. Basic theory of real-time RoS measurement, learning-based RoS model and level-set method are introduced in Section 2. The reliability of the established method is validated through comparison between numerical predictions and experimental measurements in Section 3. Conclusions are drawn in Section 4.

2. Theory

The developed numerical model consists of two parts: real-time RoS measurement as an approach to provide training data and forward modeling to predict the fire front evolution. During the RoS measurement, the RoS is defined as the fire front shift along the normal direction per unit time. Many types of numerical methods have been proposed to predict the fire front with given RoS, such as Lagrangian particle tracking [31,32], Huygens principle [33] and level-set method [34,35]. Following the work [36,37], level-set method is adopted here in the forward modeling as it can easily track the topological change of fire front.

2.1. Real-time RoS measurement

Fire fronts in wildfire images, defined as the interface between burnt and unburnt areas, can be identified with specific criteria, such as intensity, color information, and fire shape. The measured RoS is obtained from the fire front shift in two consecutive images. Fig. 1 shows the definition of parameters in the calculation. $F(x, y, t_0)$ and $F(x, y, t_0\text{-}\Delta t)$ are fire fronts at $t = t_0$ and $t_0-\Delta t$, respectively. Although fire may spread in both tangential and normal directions, the evolution of fire front is only determined by the normal RoS. For any point (x_0, y_0) at the fire front, RoS is dependent on the movement of the tangential line $L(x_0, y_0, t_0)$. Numerical procedures are listed below.

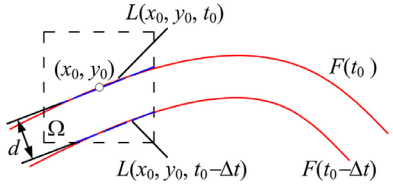

Fig. 1. Illustration of notations in the RoS measurement algorithm. $F(x, y, t_0)$: fire front at $t = t_0$; $L(x_0, y_0, t_0)$: tangential line at $(x, y) = (x_0, y_0)$; Δt: time interval between the two images; Ω: neighborhood of (x_0, y_0); $L'(x_0, y_0, t_0-\Delta t)$: best fitted line of $F(x, y, t_0-\Delta t)$ in Ω with the same slope of $L(x_0, y_0, t_0)$; d: distance between $L(x_0, y_0, t_0)$ and $L'(x_0, y_0, t_0\text{-}\Delta t)$.

(1) For a specified point (x_0, y_0) at the fire front $F(x, y, t_0)$, a linear expression, given by Eq. (1), is used to fit the front in its neighborhood Ω to get the tangent line. Normally high RoS requires large Ω to include the tangent line in the following time step.

$$ax + by = 1, \tag{1}$$

where (x, y) are the coordinates of the points at the front, a and b are two independent variables to be calculated.

(2) The tangent line moves in the normal direction with evolution of fire front. Eq. (2) is adopted to fit the new line. Note that a and b are identical to the ones in Eq. (1), as rotation and tangential movement of the line are not accounted for.

$$ax + by = c, \tag{2}$$

where c is the variable to be optimized.

(3) The RoS depends on distance between the two parallel lines described by Eqs. (1) and (2), given by

$$d = \left| \frac{1 - c}{\sqrt{a^2 + b^2}} \right|. \tag{3}$$

(4) Combined with the time interval Δt, the RoS is calculated as

$$\vec{U}(x_0, y_0) = \frac{d}{\Delta t}\left(\frac{a}{a^2 + b^2} \frac{b}{a^2 + b^2} \right). \tag{4}$$

Although $\vec{U}(x_0, y_0)$ is set to be normal to the fire front, it does not account for the sign of (1-c) in Eq. (3). The direction of $\vec{U}(x_0, y_0)$ depends on the sign of c-1. If c is smaller than 1, $\vec{U}(x_0, y_0)$will be in the opposite direction.

(5) Repeat Steps (1)–(4) for every point at the fire front to get the RoS.

(6) Since there might be noise in the RoS field due to quantization errors, numerical errors and uncertainties in determination of fire front, further smooth of RoS field is necessary to suppress the noise effect. Median filter given by Eq. (5) and average filter given by Eq. (6) are therefore performed.

$$\vec{U}'(x, y) = median\left\{\vec{U}(x - k, y - l)\right\}, (k, l \in M), \tag{5}$$

$$\vec{U}'(x, y) = \sum\nolimits_{k,l} \vec{U}(x - k, y - l)/_n, (k, l \in M), \tag{6}$$

where k and l are the indices in the neighborhood M with typical size of 5 × 5, n is the pixel number in M. Since $\vec{U}(x, y)$ only exists at the fire front, (x-k, y-l) needs to be at the fire front in both Eqs. (5) and (6) .

The accuracy of RoS measurement depends on the spatial resolution of raw fire image and time interval between two consecutive images. Appropriate spatial resolution should be employed when taking the images. Low spatial resolution would cause considerable

quantization errors, while high spatial resolution is neither needed due to irregular micro-structure of fire fronts. In a regional-scale wildfire event, a spatial resolution of about 10 m can work for the RoS measurement described here. The time interval is determined by RoS as the fire front shift in the two consecutive images can neither be too large nor small. Since the images are usually continuously captured in a real wildfire, the time interval can be set by observing the fire front movement in the images.

For a smooth fire front with large curvature radius, the RoS measurement is approximately independent on the neighborhood size as the fitted tangent line remains almost unchanged. The dependence becomes stronger for smaller curvature radius. Although setting a small neighborhood size is beneficial for enhancing the spatial resolution of RoS, it renders the RoS measurement vulnerable to the influences of irregular micro-structures of fire fronts. Therefore, the neighborhood size should be large enough to reduce the fluctuation of fire front in a real wildfire.

2.2. Forward modeling

2.2.1. RoS model

To validate the proposed method, a RoS model is required for numerically generating the fire front. Without loss of generality, Fendell's model [37] is adopted, which was developed for wind-aided wildfire spreading over level terrain.

The RoS at the fire front is given by

$$U(V,\theta)=\begin{cases}\varepsilon_0+\alpha\sqrt{V\cos^n\theta} & |\theta|\le\dfrac{\pi}{2}\\ \varepsilon_0[\beta+(1-\beta)|\sin\theta|] & |\theta|>\dfrac{\pi}{2}\end{cases}, \tag{7}$$

where ε_0 and α are parameters depending on fuel characteristics, V is the wind velocity, θ is the angle between the wind direction and the normal to the fire front, β is the ratio of the RoS at the rear ($\theta=\pi$) to that at the flanks ($\theta=\pi/2$).

Fire would advance faster over a hill with a positive slope. The RoS model is thus modified to account for the slope effect:

$$U_{slope}=U\times e^{2s}, \tag{8}$$

where s is the slope with unit of radian.

2.2.2. Eulerian level-set method

Eulerian level-set method is adopted to model the fire spread with specified RoS. Fire front is defined as the zero level set of a smooth time-dependent function $\varphi(t, x, y)$. Although $\varphi(t, x, y)$ has no physical meaning, the movement of its zero level set reveals the front evolution. For practical issues (e.g., initialization of φ, normal direction of front), it is usually convenient to use signed distance function as the level-set function $\varphi(t, x, y)$, given by

$$\varphi(t,x,y)=\begin{cases}-d_{\Gamma(t)}(x,y) & (x,y)\text{ inside the fire}\\ d_{\Gamma(t)}(x,y) & (x,y)\text{ outside the fire}\end{cases}, \tag{9}$$

where $d_{\Gamma(t)}(x, y)$ is the distance between (x, y) and the nearest point of fire front. According to the definition of distance function, normal direction of fire front can be easily identified as

$$\vec{n}=n_x\vec{i}+n_y\vec{j}=\frac{1}{|\nabla\varphi|}\left(\frac{\partial\varphi}{\partial x}\vec{i}+\frac{\partial\varphi}{\partial y}\vec{j}\right). \tag{10}$$

Meanwhile, the angle θ between the wind direction and the normal direction can also be obtained to account for wind effect. The evolution of level set function is described by

$$\frac{\partial\varphi}{\partial t}+\vec{U}\nabla\varphi=0, \tag{11}$$

where $\vec{U}$exists in the entire computation domain. Since RoS is defined only at the fire front, it needs to be extended over the domain. Here the nearest point method is adopted, where $\vec{U}$at any point in the solution domain is defined to be that of the nearest point at the front. The zero level set of new φ can then be extracted to get the new front. Note that the evolution of φ in the entire domain is unnecessary except those near the interface based on the fact that only the front needs to be tracked. Therefore, a narrow-band level-set method, where only the area near the front is updated, is adopted to reduce the computational cost.

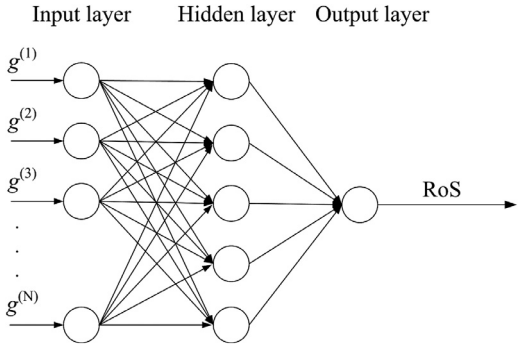

Fig. 2. Illustration of overall framework of a multilayer perceptron neural network.

2.2.3. Machine learning

As the RoS measurement can only be conducted in the burnt area, a method is required to predict the RoS in the unburnt area. In the numerical experiment, the RoS can be easily derived via Eq. (7), but in a real fire, the empirical RoS model may introduce additional error. Since the RoS measurement has already been performed at the fire front, machine learning can serve as a powerful tool to predict RoS in the unburnt area. Although deep learning has attracted much attention in recent years, it is usually employed in image processing and requires a large-scale neural network that needs more training time to update parameters according to real-time measurements. As the RoS has already been obtained, a small-scale neural network can also be capable of mapping the model parameters into RoS. Therefore, a small-scale multilayer perception neural network is employed in this paper, which greatly reduces the complexity. Fig. 2 shows the framework of the neural network. In the network, the output parameter is the measured RoS and the input parameter is a vector $\boldsymbol{g}=[g^{(1)}, g^{(2)}, \ldots, g^{(N)}]$, including wind direction, wind velocity, normal direction of fire front, environment parameters, etc. The requirements on data sets are the same as that in other data-driven works [24–31]. With the measured RoS and known input parameters, the connection weights among different neurons and neuron bias are updated by the classical back-propagating (BP) training algorithm, where no special treatment is employed to accelerate the convergence of training.

2.2.4. Numerical procedure

Meshes and model parameters are first initialized and the level set function $\varphi\ (x, y, t_0)$ is defined according to the initial condition. For an ideal circle or rectangle fire source, the level set function can be set by analytically calculating the distance between the point and the fire front. In contrast, a reinitialization procedure is needed to ensure that the level set function satisfies the definition of distance function for a real wildfire with irregular fire front. The reinitialization procedure based on the dilate operation in image processing is listed below.

(1) When $\varphi(x, y, t_0)$ is provided, the front (x_0, y_0) is the zero level set of $\varphi(x, y, t_0)$. Due to the quantization error, (x_0, y_0) is considered as the front when $\varphi(x_0-\Delta x, y_0, t_0)\ \varphi(x_0+\Delta x, y_0, t_0)< 0$ or $\varphi(x_0, y_0-\Delta y, t_0)\ \varphi(x_0, y_0+\Delta y, t_0)< 0$, where Δx and Δy are

the mesh size in the x and y direction. In a real wildfire image, the front (x_0, y_0) can be extracted as the boundary of burnt area. The point set of (x_0, y_0) is saved in an array $Point[N]$. $\varphi(x, y, t_0)$ at other points in the computation domain is assigned to be $W\text{sgn}[\varphi(x, y, t_0)]$, where $\text{sgn}(\varphi)$ is the sign function which equals 1 if $\varphi > 0$ and -1 if $\varphi < 0$, W is the width of the narrow band. Large W is required for high RoS so that fire front would not spread out of the narrow band at the next time step.

(2) For each point (x_0, y_0) in $Point[N]$, dilate operation is performed with increased radius until reaching the boundary of narrow band. When a new point (x_1, y_1) is reached, its distance function from (x_0, y_0) is $\varphi_1(x_1, y_1) = \text{sgn}[\varphi(x_1, y_1)]\sqrt{(x_1 - x_0)^2 + (y_1 - y_0)^2}$. If $|\varphi_1(x_1, y_1)|$ is smaller than the absolute value of current level set function $|\varphi(x_1, y_1)|$, $\varphi(x_1, y_1) = \varphi_1(x_1, y_1)$. To further extend the RoS at the front to the narrow band, two new two-dimensional arrays $Pointx[x, y]$ and $Pointy[x, y]$ are employed to store the position coordinates of the nearest point at the front for each point in the narrow band by setting $Pointx[x_1, y_1] = x_0$ and $Pointy[x_1, y_1] = y_0$.

(3) After the discretization of computation domain, quantization noise in the level set function $\varphi(x, y, t_0)$ becomes inevitable. An average filter is applied to $\varphi(x, y, t_0)$ since $\varphi(x, y, t_0)$ should be inherently smooth.

After the reinitialization, Eq. (11) needs to be solved to derive the fire front with the measured RoS. As Eq. (11) requires $\vec{U}$ in the entire domain, the RoS needs to be extended from fire front. Since the position of nearest point at the fire front for each point in the narrow band is stored in $Pointx[x, y]$ and $Pointy[x, y]$, $\vec{U}(x_1, y_1)$ is defined to be the value of $\vec{U}(Pointx[x_1, y_1], Pointy[x_1, y_1])$.

Finite difference method is then adopted to numerically solve Eq. (11) to obtain the level set function at the next time step $\varphi(x, y, t_0 + \Delta t)$, as given by Eq. (12).

$$\left(\frac{\partial \varphi}{\partial x}\right)_{i,j}^{n} = \frac{\varphi_{i+1,j}^{n} - \varphi_{i-1,j}^{n}}{2\Delta x}, \left(\frac{\partial \varphi}{\partial y}\right)_{i,j}^{n} = \frac{\varphi_{i,j+1}^{n} - \varphi_{i,j-1}^{n}}{2\Delta y}, \left(\frac{\partial \varphi}{\partial t}\right)_{i,j}^{n} = \frac{\varphi_{i,j}^{n+1} - \varphi_{i,j}^{n}}{\Delta t} \tag{12}$$

where Δt is the time interval. Substituting Eq. (12) into Eq. (11), the level set function at the next time step is given by

$$\varphi_{i,j}^{n+1} = \varphi_{i,j}^{n} - \Delta t\left[U_y\left(\frac{\partial \varphi}{\partial y}\right)_{i,j}^{n} + U_x\left(\frac{\partial \varphi}{\partial x}\right)_{i,j}^{n}\right], \tag{13}$$

where U_x and U_y are, respectively, the x and y components of $\vec{U}(x, y)$.

To ensure numerical convergence, the time interval Δt has to satisfy the Courant–Friedrichs–Lewy condition, given by

$$\frac{U_x \Delta t}{\Delta x} + \frac{U_y \Delta t}{\Delta y} < 1. \tag{14}$$

The overall flowchart for the proposed learning-based wildfire spread model is illustrated in Fig. 3. If two consecutive simulated or experimental fire fronts are available, the RoS along the normal direction is first obtained by fitting tangent lines and calculating normal displacement at every point. The measured RoS is then input into a neural network with localized slope and normal direction, where the classical back-propagation training algorithm is employed to automatically adjust the network parameters. The narrow-band Eulerian level-set method finally predicts short-term fire spread with the RoS in unburnt area provided by the neural network.

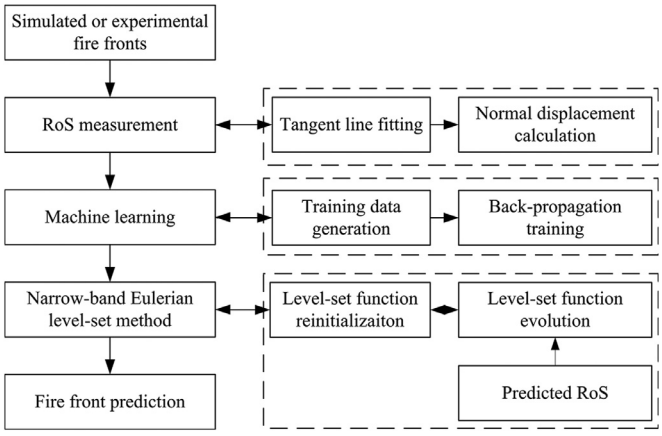

Fig. 3. Flowchart of the learning-based prediction of wildfire spreading model.

3. Results

In this section, the validations of forward modeling, RoS measurement, and machine learning technique are individually implemented and prediction of a real scale shrubland fire is conducted. The forward modeling is coded in C++ language, while the RoS measurement and machine learning are conducted in Matlab. The RoS prediction is transferred from Matlab to C++ program through Matlab engine. A personal computer with a CPU of Intel(R) Core(TM) i5-4200U @ 1.60 GHz and 8.00 GB RAM is employed in the simulations.

3.1. Validation of the level-set method

The creditability of forward modeling was firstly examined with ideal fire spread. The initial source is a circular fire with a radius of 100 m. The RoS and width W of the narrow band are respectively set to be 1 m s^{-1} and 20 m. No wind is applied in this case and the fire front shape should keep unchanged. Therefore, the radii of fire fronts at different times should be $R = (200 + t)$ m. It takes about 180 s to simulate the fire spread from $t = 0$ s to 200 s with Δt of 0.1 s and Δx, Δy of 1 m. Fig. 4(a) gives the reconstructing narrow-band level set function at $t = 120$ s. As expected, the level set function corresponds to the distance function in the narrow band and in constant outside. The fire fronts at different times are extracted and fitted into a circle by the least-square method. The radii of the circles are 200.0 m, 240.0 m, 279.8 m, 319.7 m, 359.8 m and 399.8 m at $t = 0$ s, 40 s, 80 s, 120 s, 160 sand 200 s, respectively, as shown in Fig. 4(b). The relative errors, which may come from the quantification error, are less than 0.5% compared with theoretical value, demonstrating that the narrow-band level set method can precisely predict the fire front spread process for given RoS.

Influences of wind and slope are then examined. In the simulation, the wind is assumed to be in the positive x-direction with a speed of 1 m s^{-1}. Other related parameters are $\varepsilon_0 = 1$, $\alpha = 1$, $n = 3$, $\beta = 0.5$, respectively. The initial fire front is the same as that in Fig. 4(b). Simulation results are given in Fig. 4(c). Due to wind influences, the fire front is no longer circular but features a more complicated shape dependent on the RoS model given by Eq. (7), which elongates when $\theta < |\pi/2|$ and shrinks when $\theta < |\pi/2|$. In Eq. (7), the RoS at $\theta = 0°$ and 180° are, respectively, 2 m s^{-1} and 0.5 m s^{-1}. The theoretical x positions of fire front at $\theta = 0°$ and 180° are respectively $x = (600 + 2t)$ m and $x = (400 - 0.5t)$ m, which can also be validated in Fig. 4(c). An idealized uphill with a slope of $\pi/8$ is introduced between $x \in$ [700 m, 800 m] in Fig. 4(d). The fire spread is accelerated in this region according to Eq. (8).

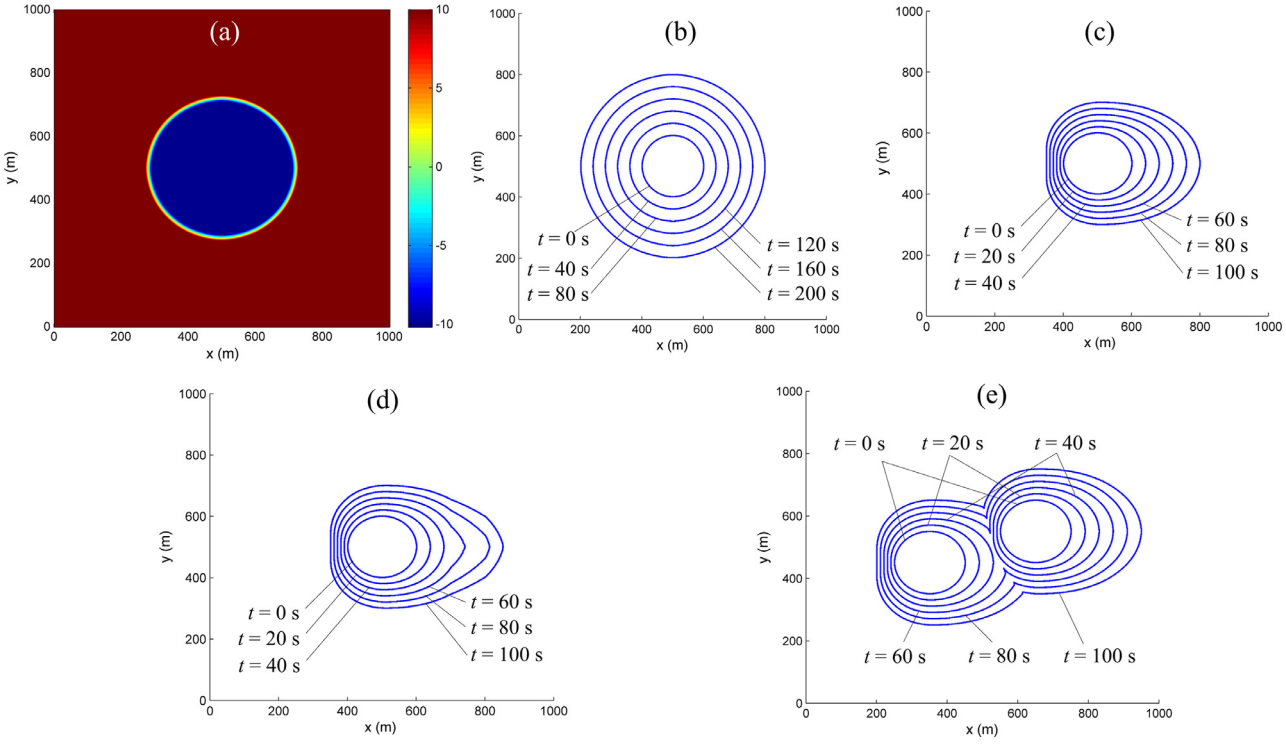

Fig. 4. (a) Narrow-band level set function at t = 120 s. Fire fronts under (b) no wind, (c) wind influence, (d) wind and slope influences at different times. (e) Evolution of merged two fire fronts at different times.

One of the advantages of the level-set method is that no additional treatment is needed to deal with two fire ignitions. As shown in Fig. 4(e), the initial two fire fronts are separately located at (350 m, 450 m) and (650 m, 550 m) and are merged during the spreading. As expected, the front disappears in the merging area while other segments are not affected. The fire front near the intersection is smooth in the simulation, similar to that in the real fire, demonstrating that the method is capable of simulating topological change of fire front.

3.2. Validation of RoS measurement

The RoS measurement algorithm is examined to ensure that it provides reliable data sets for further machine learning work. Numerically generated fire fronts in Fig. 4(c) are employed as the raw data and the RoS measurement is compared with the theoretical value used in the forward modeling. The size of neighborhood Ω is 31 m $\times$ 31 m. To examine the dependence of RoS measurement on time interval, Δt = 10 s, 20 s, and 30 s are individually used in the calculation. Fig. 5 gives the results of theoretical RoS and relative RoS measurement errors with different Δt at t = 100 s. Although the absolute RoS measurement error barely changes along the fire front, the relative error is smaller near $\theta = 0°$ than $\theta = \pm 180°$ as the absolute value of RoS is much higher near $\theta = 0°$. As the RoS is defined to be the derivative of fire front shift with respect to t, a smaller Δt should theoretically result in higher precision. However, the fire front position in a real fire can hardly be precisely determined and a smaller Δt may introduce significant RoS uncertainty. Therefore, a considerable fire front shift should be observed during the time interval. Nevertheless, the relative measurement error is less than 6% in all the three cases, demonstrating the feasibility of the proposed method.

The RoS measurement is subsequently applied on fire fronts in Fig. 4(d), results of which are shown in Fig. 6. Similar trend of relative error dependency on time intervals is found. An abrupt

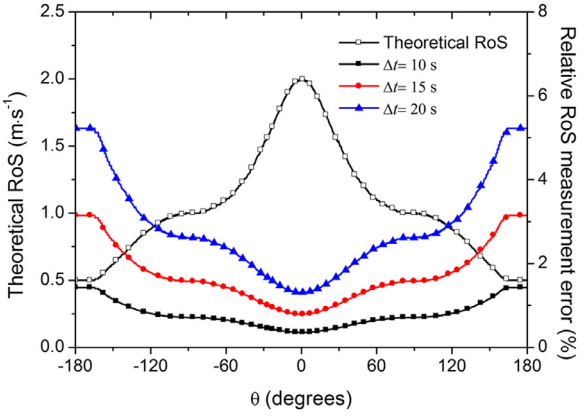

Fig. 5. Theoretical RoS and relative errors of RoS measurement at t = 100 s with three different time intervals under the influences of wind.

increase of measurement error is observed at x = 700 m and 800 m since the theoretical RoS depends on the local slope that varies intensively at the intersection of uphill and level terrain, while the measured one is the average value of the neighborhood. The smooth of RoS would be helpful in reducing noise influences for a real fire.

3.3. Validation of learning-based RoS model

Machine learning aims at establishing the relationship between RoS model parameters and RoS measurements. In this study, the input and output parameters are respectively the normal direction of fire front and RoS. If other relevant parameters, such as fuel types, moisture and slope, are available, they can also be included in the input parameters. The sample set was provided by theoretical RoS with the same parameters as that in Fig. 4(c). Computation

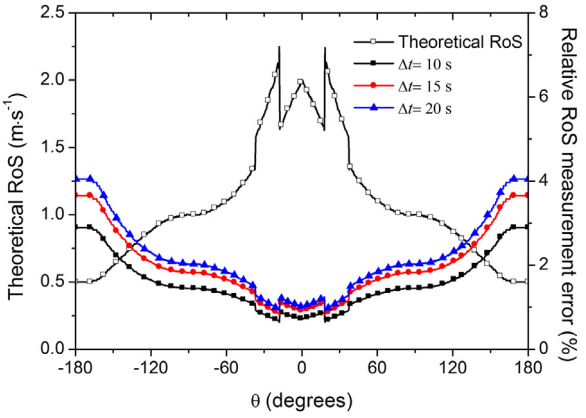

Fig. 6. Theoretical RoS and relative errors of RoS measurement at with three different time intervals $t = 100$ s under the combined influence of wind and slope influences.

of machine learning is conducted via the neural network toolbox. Ten neurons with *tansig* transfer function are used in the hidden layer, while the transfer function for the output neuron is defined to be *purelin* function. Built-in functions *trainlm* and *learngdm* in the toolbox are employed to train the network and update the parameters. The default mean squared error function is adopted as the loss function.

Machine learning of RoS field with both zero and nonzero slopes are examined. Results are shown in Fig. 7. In Fig. 7(a), only the angle θ between the normal direction of fire front and wind direction is input into the neural network. In Fig. 7(b), slope influences are further included in the input layer, defined as

$$s = \begin{cases} \pi/8 & 30^\circ < |\theta| < 70^\circ \\ 0 & Otherwise \end{cases}. \tag{15}$$

RoS with an angle interval of 0.5° given by Eqs. (7) and (8) are used in the training. The model parameters are the same as that in Fig. 4(c). The maximum iteration number is set to be 2000. For this small-scale network, the training usually takes about 5 s, which can be further accelerated by employing new types of machine learning techniques, such as extreme learning machine [38]. By comparison, wildfire spread simulation needs to be conducted multiple times to optimize the model parameters by the genetic algorithm in Ref. [30], which suffers from low computational efficiency. After training, the neural network is tested with randomized normal direction. In both cases, good agreements between predicted and theoretical RoS are observed and the average relative errors are less than 1%, demonstrating that machine learning is a reliable approach to model RoS. Although only the wind and slope are employed as input parameters in the test, more neutrons could be added into the input layer to include the influence of more environmental parameters in a real fire at the cost of larger data sets. Typical convergence rate evolution over iteration in the training is given in Fig. 8. As expected, the mean squared error converges fast at the beginning but changes little after 100 iterations. Note that it is unnecessary to employ more hidden neurons for reducing the final mean squared error, as more hidden neurons require more training data to avoid overfitting that may lead to poor generalization performance.

3.4. Fire spread prediction

To predict wildfire spread, the fire front evolution needs to be modeled with future RoS determined by the measured RoS. In the previous data-driven works, future RoS was usually determined by an empirical model with parameters obtained by optimizing the

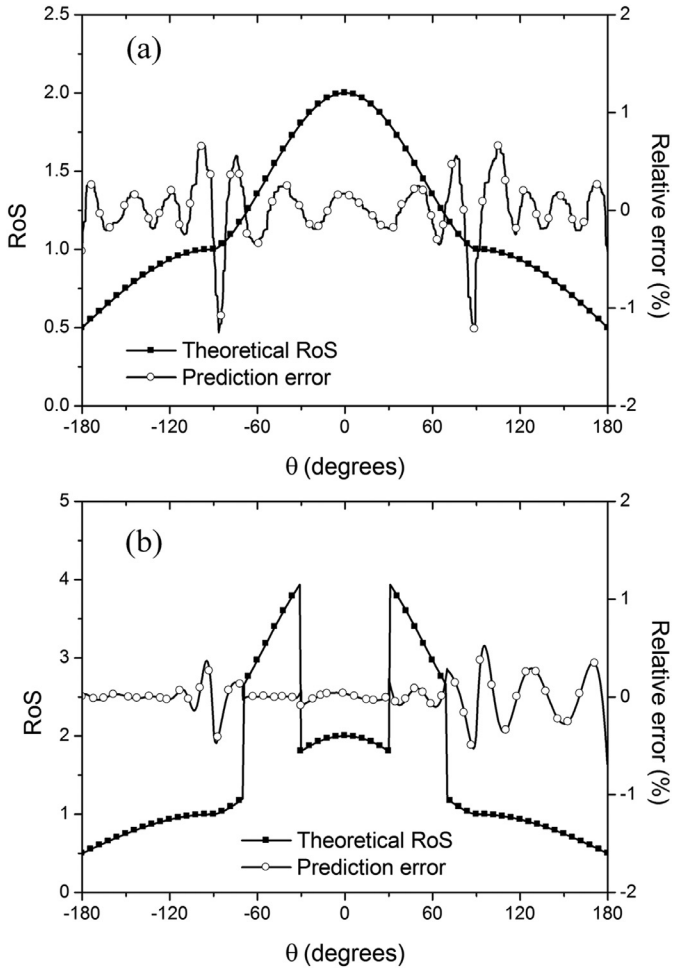

Fig. 7. Prediction errors of RoS based on machine learning. (a) RoS under no slope condition; (b) RoS affected by non-uniform slope distribution.

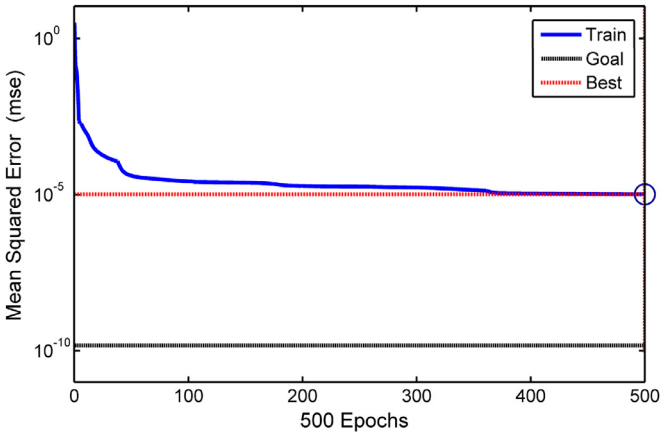

Fig. 8. Mean squared error evolution in the training.

deviation between observed and simulated fire fronts. However, it is typically difficult to select an appropriate empirical model capable of precisely giving the RoS for a real wildfire. As an improvement, machine learning is adopted to avoid the use of explicit empirical model. Fig. 9 depicts the comparison between predicted fire front and theoretical fire fronts shown in Fig. 4(c). Relative error of distance from (500 m, 500 m) is adopted as a metric to reveal the deviation between predicted and theoretical fire fronts.

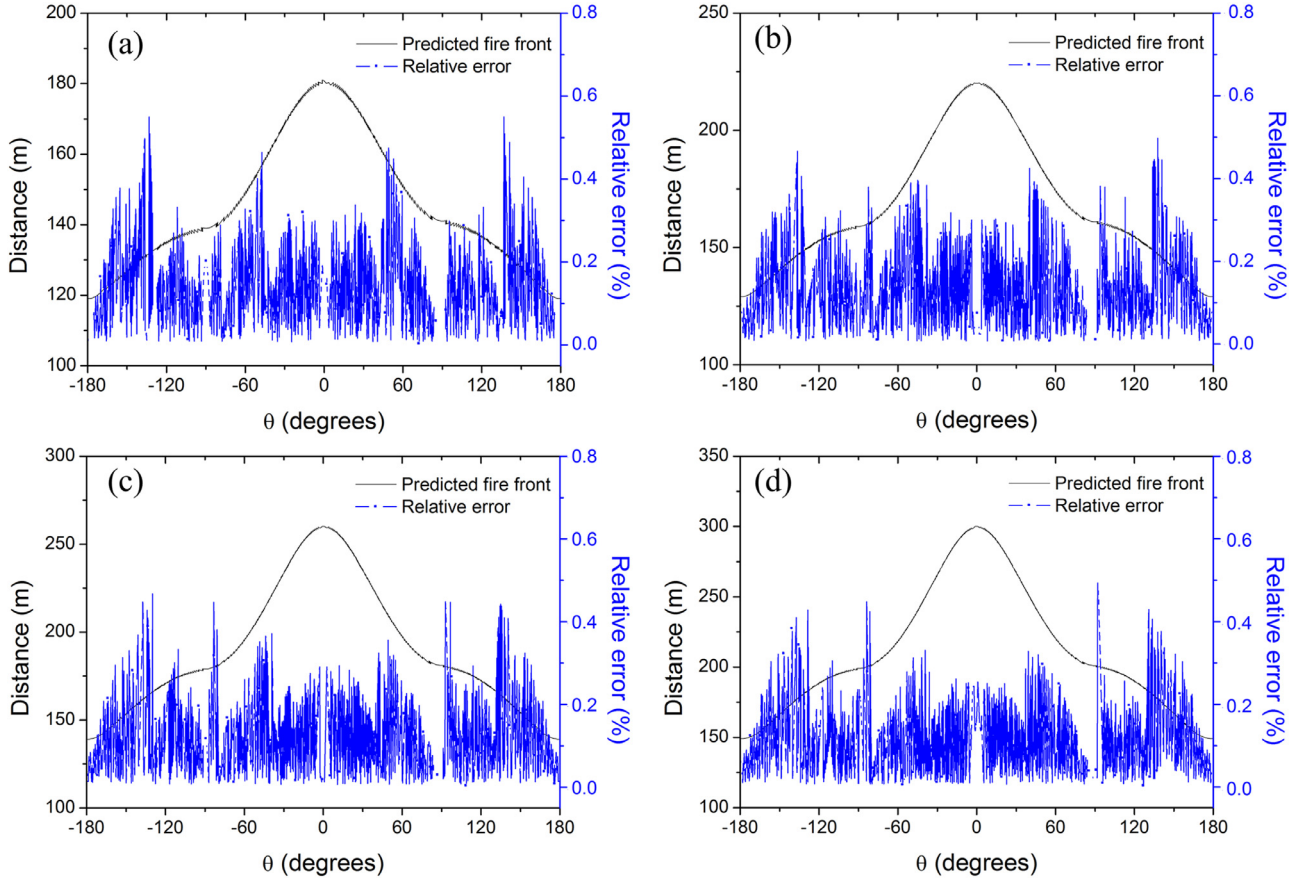

Fig. 9. Fire front predictions corresponding to the simulation in Fig. 4(c). (a) $t = 40$ s, (b) $t = 60$ s, (c) $t = 80$ s, and (d) $t = 100$ s.

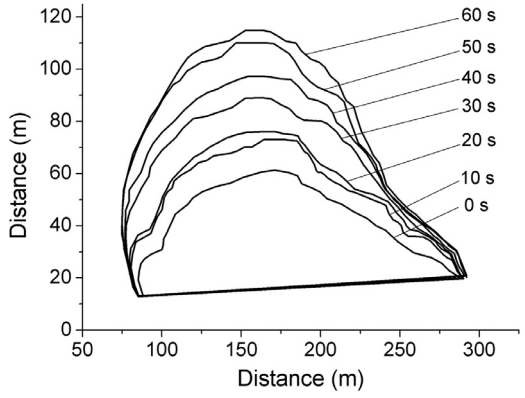

Fig. 10. Fire fronts at different times from $t = 0$ s to $t = 60$ s with 10 s time intervals in the real scale shrubland fire experiment [32].

RoS at $t = 20$ s is first calculated with the fire fronts at $t = 20$ s and $t = 0$ s and then adopted to train the neural network. The RoS at fire fronts is finally extended in the narrow-band region by the nearest point method at each time step. The relative distance errors are always smaller than 0.8%, indicating that the method is capable of predicting short-term wildfire spreading with idealized RoS.

The proposed method is then applied to a real-scale shrubland fire experiment. Details of the experiment can be found in Rios et al. [32]. Fig. 10 shows the extracted fire fronts at different times. Compared with ideal experiments, the experimental data is much more irregular and the RoS can hardly be obtained through an idealized RoS model. As the data is collected for every 10 s, the fire front change during the time interval is relatively large. To keep the two fronts inside Ω (Fig. 1) for RoS measurement, the size of Ω is set to be 70 m × 70 m. Fire front positions in a smaller neighborhood with size of 5 m × 5 m is used to fit the tangent line. RoS at $t = 20$ s, 30 s, 40 s, 50 s and 60 s are calculated with time intervals of 10 s and 20 s. As the fire front shifts in every 10 s change a lot, the retrieved RoS with different time intervals also differ a lot. Fig. 11 gives the results of RoS at different times, where θ is defined to be the angle in a polar coordinate system with $(x_c, y_c) = (186\text{ m}, 17\text{ m})$ as the origin. Since fire fronts only exists in the region with $y > y_c$, the range of θ is approximately to be (0°, 180°). Note that θ in Fig. 11 is different from that in Fendell's model defined to be the angle between wind direction and normal direction of fire front. Based on the fact that the RoS calculated with $\Delta t = 20$ s is a smoothed value of that calculated with $\Delta t = 10$ s, $\Delta t = 20$ s is employed in the RoS measurement for further prediction.

As more detailed information of the experiment and environment (slope, temperature, moisture, etc.) is unknown, only the normal direction of fire front is accounted for in the machine learning. Fig. 12(a) gives the measured RoS with $\Delta t = 20$ s at $t = 30$ s and its fitted results by machine learning. Unlike Fig. 11, the x-coordinate in Fig. 12(a) is the angle between the x-axis and normal direction of fire front as required by Fendell's model. As fire fronts at different positions may have the same normal direction, the measured RoS oscillates intensively between (0°, 30°) and (150°, 180°). By comparison, the fitted results by neural network is much more smoothed, which helps to reduce the influence of measurement noise. Prediction of fire fronts after $t = 30$ s with lead time of 30 s is given in Fig. 12(b). The predicted fire fronts generally agree with the observed one, but there are still some errors

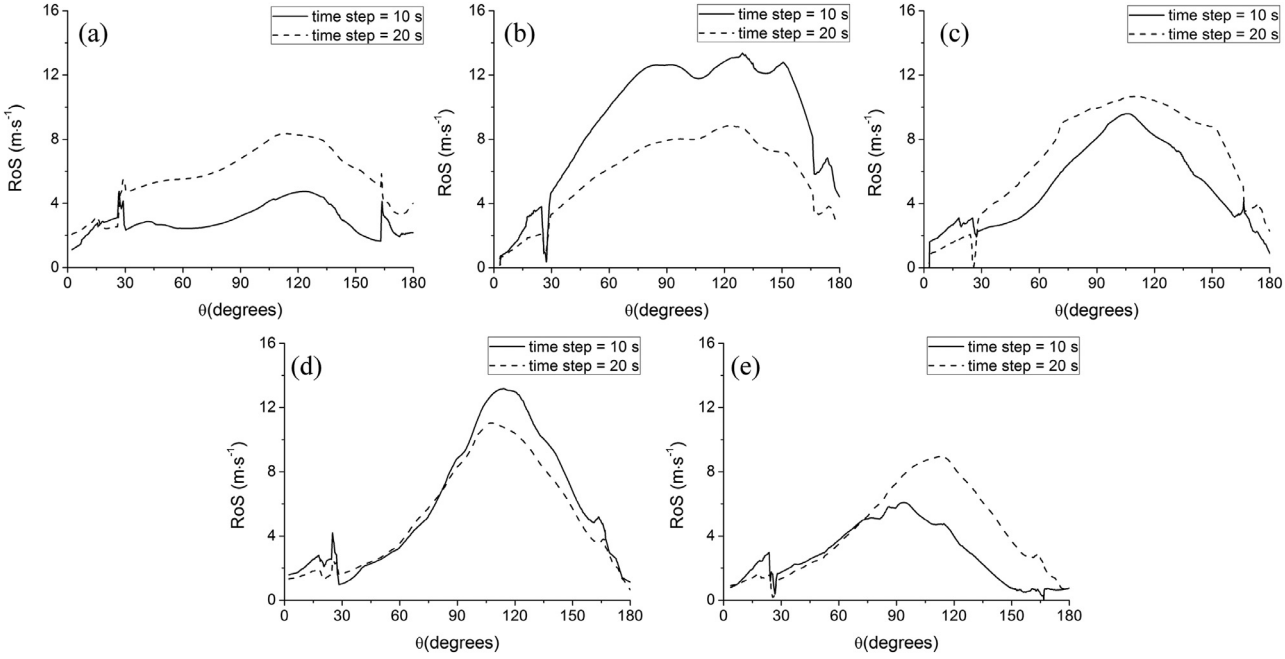

Fig. 11. RoS at t = (a) 20 s, (b) 30 s, (c) 40 s, (d) 50 s, and (e) 60 s calculated with time interval Δt = 10 s and 20 s.

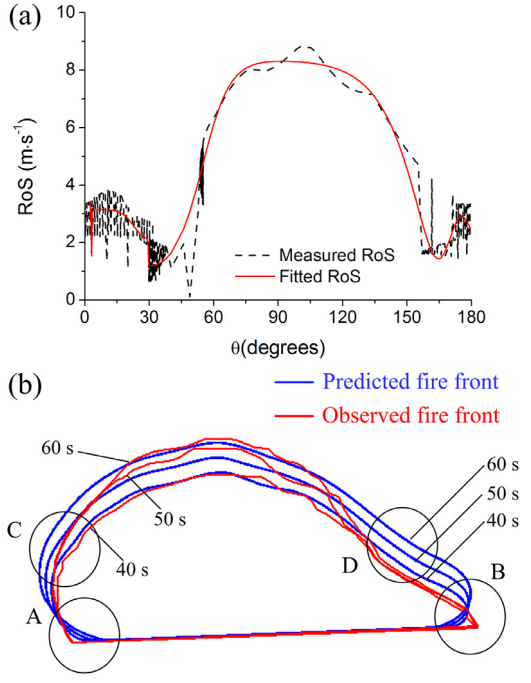

Fig. 12. (a) Comparison between measured and fitted RoS at t = 30 s. (b) Comparison of predicted and observed fire fronts at t = 40 s, 50 s and 60 s.

between the two. In the A and B regions, the observed fire front is approximately fixed but the predicted fire front changes due to the reinitialization of level set function, which is intrinsically a smooth filter. Nevertheless, no systematic error is introduced for a real wildfire where fire fronts are uncontrolled. In the C and D regions, the proposed model overestimates the fire front spread because that the RoS in these regions significantly decreases when $t > 40$ s due to the variables that has not been considered in the machiney learning.

Compared with simulated data, the deviation is much larger for experimental data because only the influences of normal direction of fire front on RoS are considered. However, in a real wildfire, there are many parameters that may affect the RoS. More environment and fuel parameters should be accounted for and included in the input layer to improve the prediction accuracy. Although the preliminary results presented in this work show that machine learning can be a tool to overcome the limitation of empirical RoS model, there is no doubt that machine learning is not a universal method that can solve every problem in the wildfire spread model. To exploit the potential of machine learning, related parameters (wind, slope, fuel, etc.) need to be accurately measured, which still requires a lot of work on remote sensing, image processing, and environmental metrology.

4. Conclusions

This work reports a novel data-driven model for short-time prediction of wildfire spread. Unlike conventional approach where model parameters are optimized to minimize the deviation between measured and numerically predicted fire front, real-time RoS measurements are performed to update the predicted RoS, which can improve the computationally efficiency by avoiding time-consuming optimization. Machine learning is adopted to provide RoS estimation in the unburnt area without assumption of specified empirical RoS model. Narrow-band level-set method is employed to predict the fire front evolution. The proposed method is validated with numerically generated data and observed fire front of controlled shrubland fire, showing that it is capable of predicting short-term wildfire spread. In the current work, only the normal direction of fire front is used in the training of neural work. More environmental and fuel parameters can be included in the input layer to improve the prediction accuracy in the future.

Declaration of Competing Interest

The authors declare that they have no known competing financial interests or personal relationships that could have appeared to influence the work reported in this paper.

Acknowledgments

Our deepest gratitude goes to the anonymous reviewers for their careful work and thoughtful suggestions that have helped improve this paper substantially. This work is supported by the National Key R D Program of China (2017YFD0600106-4); Nanjing Forest Police College Pre-research Project (LGY201801); the Qing Lan Project, the Priority Academic Program Development of Jiangsu Higher Education Institutions of China; National Natural Science Foundation of China (31872705, 61605081). The authors deeply appreciate the support.

References

[1] M. Gennaro, Y. Billaud, Y. Pizzo, et al., Real-time wildland fire spread modeling using tabulated flame properties, Fire Saf. J. 91 (2017) 872–881.
[2] S. Yassemi, S. Dragićević, M. Schmidt, Design and implementation of an integrated GIS-based cellular automata model to characterize forest fire behaviour, Ecol. Model. 210 (2008) 71–84.
[3] L. Holsinger, S.A. Parks, C. Miller, Weather, fuels, and topography impede wildland fire spread in western US landscapes, Forest Ecol. Manag. 380 (2016) 59–69.
[4] D.E. Calkin, M.P. Thompson, M.A. Finney, Negative consequences of positive feedbacks in US wildfire management, Forest Ecosyst. 2 (2015) 1–9.
[5] X. Cavard, J.F. Boucher, Y. Bergeron, Vegetation and topography interact with weather to drive the spatial distribution of wildfires in the eastern boreal forest of Canada, Int. J. Wildland Fire 24 (2015) 391–406.
[6] B.M. Collins, J.D. Miller, A.E. Thode, et al., Interactions among wildland fires in a long-established Sierra Nevada natural fire area, Ecosystems 12 (2009) 114–128.
[7] R. Linn, J. Reisner, J. Colman, et al., Studying wildfire behavior using FIRETEC, Int. J. Wildland Fire 11 (2002) 233–246.
[8] W. Mell, M. Jenkins, J. Gould, et al., A physics-based approach to modelling grassland fires, Int. J. Wildland Fire 16 (2007) 1–22.
[9] E. Mueller, W. Mell, A. Simeoni, Large eddy simulation of forest canopy flow for wildland fire modeling, Can. J. Forest Res. 44 (12) (2014) 1534–1544.
[10] M. Finney, FARSITE: fire area simulator – model development and evaluation, Technical report, US Department of Agriculture, Forest Service, Rocky Mountain Research Station, USA, 1998.
[11] A.G. McArthur, Weather and Grassland Fire behavior, Forestry and Timber Bureau, Department of National Development, Commonwealth of Australia, 1966.
[12] R.C. Rothermel. A mathematical model for predicting fire spread in wildland fuels, USDA forest service, intermountain forest and range experiment station, Ogden, research paper, INT-115, 1972.
[13] B.J. Stocks, M.E. Alexander, R. Lanoville, Overview of the international crown fire modelling experiment (ICFME), Can. J. Forest Res. 34 (2004) 1543–1547.
[14] Z. Wang, Current forest fire danger rating system, J. Nat. Disasters 1 (3) (1992) 39–44 in Chinese.
[15] M. Finney, J. Cohen, S. McAllister, et al., On the need for a theory of wildland fire spread, Int. J. Wildland Fire 22 (2013) 25–36.
[16] M.G. Cruz, M.E. Alexander, Uncertainty associated with model predictions of surface and crown fire rates of spread, Environ. Model. Softw. 47 (2013) 16–28.
[17] A. Sullivan, Wildland surface fire spread modeling, 1990-2007. 2: empirical and quasi-empirical models, Int. J. Wildland Fire 18 (2009) 369–386.
[18] M. Pierro, M.D. Felice, E. Maggioni, et al., Data-driven upscaling methods for regional photovoltaic power estimation and forecast using satellite and numerical weather prediction data, Sol. Energy 158 (2017) 1026–1038.
[19] M. Reder, N.Y. Yürüşen, J.J. Melero, Data-driven learning framework for associating weather conditions and wind turbine failures, Reliab. Eng. Syst. Saf. 169 (2018) 554–569.
[20] N. Kristic, W. Yuchi, H.C. Ho, et al., The heat exposure integrated deprivation index (HEIDI): a data-driven approach to quantifying neighborhood risk during extreme hot weather, Environ. Int. 109 (2017) 42–52.
[21] R. Paugam, M. Wooster, G. Roberts, Use of handheld thermal imager data for airborne mapping of fire radiative power and energy and flame front rate of spread, IEEE Geosci. Remote. Sens. Mag. 51 (2013) 3385–3399.
[22] M. Valero, O. Rios, E. Pastor, et al., Automated location of active fire perimeters in aerial infrared imaging using unsupervised edge detectors, Int. J. Wildland Fire 27 (4) (2018) 241–256.
[23] L.F. Gonzalez, G.A. Montes, E. Puig, et al., Unmanned aerial vehicles (UAVs) and artificial intelligence revolutionizing wildlife monitoring and conservation, Sensors 16 (1) (2016) 97.
[24] J. Mandel, L.S. Bennethus, J.D. Beezley, et al., A wildland fire model with data assimilation, Math. Comput. Simulat 79 (3) (2008) 584–606.
[25] J. Mandel, J.D. Beezley, J.L. Coen, et al., Data assimilation for wildland fires: ensemble Kalman filters in coupled atmosphere-surface models, IEEE Contr. Syst. Mag 29 (3) (2009) 47–65.
[26] M.C. Rochoux, B. Delmotte, B. Cuenot, S. Ricci, A. Trouvé, Regional-scale simulations of wildland fire spread informed by real-time flame front observations, P. Combust. Inst. 34 (2013) 2641–2647.
[27] C. Zhang, M.C. Rochoux, W. Tang, et al., Evaluation of a data-driven wildland fire spread forecast model with spatially-distributed parameter estimation in simulations of the fireflux I field-scale experiment, Fire Safety J 91 (2017) 758–767.
[28] C. Zhang, A. Collin, P. Moireau, et al., Front shape similarity measure for data–driven simulations of wildland fire spread based on state estimation: application to the RXCADRE field-scale experiment, P. Combust. Inst. 37 (3) (2019) 4201–4209.
[29] M. Denham, K. Wendt, G. Bianchini, et al., Dynamic data-driven genetic algorithm for forest fire spread prediction, J. Comput. Sci. 3 (5) (2012) 398–404.
[30] C. Lautenberger, Wildland fire modeling with an Eulerian level set method and automated calibration, Fire Safety J 62 (2013) 289–298.
[31] O. Rios, W. Jahn, G. Rein, Forecasting wind-driven wildfires using an inverse modelling approach, Nat. Hazard Earth Sys 14 (6) (2014) 1491–1503.
[32] O. Rios, E. Pastor, M.M. Valero, et al., Short-term fire front spread prediction using inverse modelling and airborne infrared images, Int. J. Wildland Fire 25 (10) (2016) 1033–1047.
[33] I. Knight, J. Coleman, A fire perimeter expansion algorithm-based on Huygens wavelet propagation, Int. J. Wildland Fire 3 (2) (1993) 73–84.
[34] A.S. Bova, E.M. William, C.M. Hoffman, A comparison of level set and marker methods for the simulation of wildland fire front propagation, Int. J. Wildland Fire 25 (2) (2015) 229–241.
[35] R.G. Rehm, R.J. McDermott. Fire front propagation using the level set method, NIST Technical Note 1611, 2009.
[36] F.E. Fendell, M.F. Wolff, Forest Fires – Behavior and Ecological Effects, Academic Press, 2001.
[37] V. Mallet, D.E. Keyes, F.E. Fendell, Modeling wildland fire propagation with level set methods, Comput. Math. Appl. 57 (2009) 1089–1101.
[38] G. Huang, Q. Zhu, C. Siew, Extreme learning machine: theory and applications, Neurocomputing 70 (1–3) (2006) 489–501.